Charge and dielectric response to terahertz pulses in the charge-ordered phase of α-(BEDT-TTF)_{2}I_{3}

Shinnosuke Kuniki, Shu Ohmura, and Akira Takahashi

Phys. Rev. B **98**, 165149 — Published 30 October 2018

DOI: 10.1103/PhysRevB.98.165149

Charge and dielectric response to THz pulse in the charge ordered phase of α-(BEDT-TTF)$_2$I$_3$

Shinnosuke Kuniki, Shu Ohmura, and Akira Takahashi*

Graduate School of Engineering, Nagoya Institute of Technology,

Gokiso-Cho, Showa-ku, Nagoya 466-8555, Japan

(Dated: September 13, 2018)

Abstract

We investigated the dielectric properties of the charge-ordered phase of α-(BEDT-TTF)$_2$I$_3$ using exact numerical calculations of an extended Hubbard model. The electronic contribution to the electric polarization (electronic polarization) $\bar{\boldsymbol{P}}$ of the charge-ordered ground state is obtained by directly calculating the current when transfer integrals were changed adiabatically from symmetric integrals to integrals for the charge-ordered phase without inversion symmetry. The angle of $\bar{\boldsymbol{P}}$ from the positive $b-$axis is 36°, which is consistent with experimental results and previous theoretical results based on density functional theory. Furthermore, we numerically calculated the dynamics induced by terahertz (THz) pulse excitation. Both the THz-pulse induced variation of the electronic polarization magnitude and that of the charge disproportionation that shows the charge-order amplitude, are largest when the electric field of the THz pulse and $\bar{\boldsymbol{P}}$ have almost the same direction. This originates from the charge transfer through bond b2$'$ being dominant in both the adiabatic flow of current and THz pulse excitation. These results reproduce important features of experimental results of THz-pulse induced dynamics.

I. INTRODUCTION

Ferroelectric materials are widely used in various devices, such as random-access memory devices, capacitors, sensors, piezoelectric actuators, and optical devices.[1–3] In conventional ferroelectrics, electric polarization is governed by the rotation of polar molecules (order–disorder type) or the displacement of ions (displacive type), and the typical time constants of polarization change vary from microseconds to milliseconds. If the ferroelectric polarization could be controlled in the picosecond time domain, ferroelectric materials could be used for advanced switching devices. Recently, ferroelectricity that arises from electron transfer, which is termed electronic ferroelectricity,[4–6] has been observed in various materials, such as multiferroics,[7–14] transition metal oxides,[15–17] and organic molecular compounds,[18–37] and much faster polarization switching is expected for the new type of ferroelectricity.[5,6]

This paper focuses on α-(BEDT-TTF)$_2$I$_3$ (BEDT-TTF: bis[ethylenedithio]-tetrathiafulvalene) among various electronic ferroelectrics. The charge-transfer salts (BEDT-TTF)$_2$X (X: a monovalent anion) can be described as quasi-two-dimensional strongly correlated electron systems with a quarter-filled valence band in the hole picture. As a result of the strong Coulomb interaction, α-(BEDT-TTF)$_2$I$_3$ exhibits charge-ordering transition and a horizontal charge order forms below the transition temperature.[26–28,38–46] We show the lattice structure of α-(BEDT-TTF)$_2$I$_3$ in Fig. 1. In the charge-ordered phase, the crystal symmetry is $P1$ with no inversion symmetry, and there are crystallographically 4 nonequivalent sites and 12 nonequivalent bonds. They are labeled as indicated in Fig. 1. Sites A and B (A$'$ and C) are charge rich (charge poor) in the horizontal charge-ordered state.

The generation of ferroelectric polarization in the charge-ordered phase has been shown by optical second-harmonic-generation (SHG) measurement.[26,27] In the metallic phase above the transition temperature, the lattice structure has an inversion symmetry, and sites A and A$'$, bonds b1–b4 and b1$'$–b4$'$, and bonds a1 and a1$'$ are equivalent. Because site A (A$'$) becomes charge rich (charge poor) as a result of transition to the charge-ordered phase, it has been considered that ferroelectric polarization is parallel to the $a-$axis.[26] However, the polarization direction cannot be determined from the second-harmonic measurement. The dielectric response to the electric field perpendicular to the two-dimensional planes has been investigated, providing evidence for ferroelectricity of the charge-ordered phase.[28]

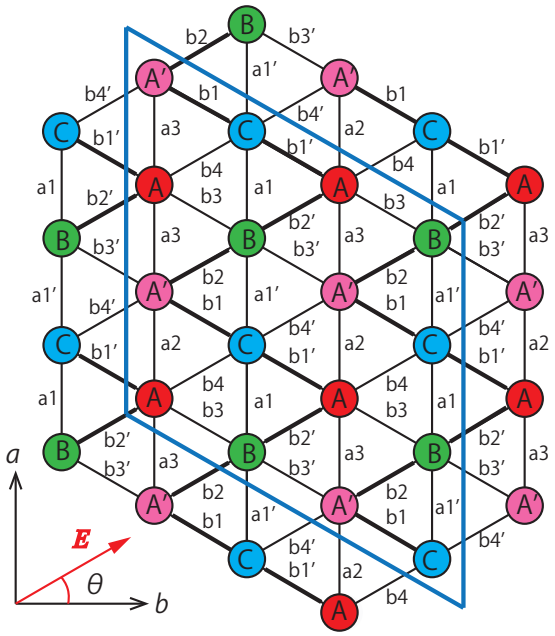

FIG. 1: (Color online) Anisotropic triangular lattices of the charge-ordered phase of α-(BEDT-TTF)$_2$I$_3$. The blue square encloses a 4×4 cluster.

However, it is difficult to investigate the in-plane dielectric response because of the low in-plane resistivity,[47] and in-plane dielectric properties including the polarization direction have not been clarified.

It has been shown, in the case of tetrathiafulvalene-p-chloranil (TTF-CA), that a terahertz (THz) pulse is a powerful tool to investigate the ultrafast dielectric response of electronic ferroelectrics.[48] Yamakawa *et al.* recently carried out THz-pump optical-probe and SHG-probe measurements on the charge-ordered phase of α-(BEDT-TTF)$_2$I$_3$ and obtained the following results.[49] The time profile of the THz-pulse-induced changes $\Delta I_{\rm SHG}/I_{\rm SHG}$ of the SHG intensity $I_{\rm SHG}$ is in good agreement with the normalized THz waveforms. The nonlinear current flow is induced by static electric fields larger than about 100 V/cm,[50,51] but the linear response occurs to THz fields at least up to 60 kV/cm. This sub-picosecond change in $\Delta I_{\rm SHG}$ is much faster than relevant lattice motions, which have the time scale of 1 picosecond,[52] and this shows that $\Delta I_{\rm SHG}$ originates from the pulse-induced modulation ΔP of the magnitude of ferroelectric polarization per unit cell $\bar{\boldsymbol{P}}$. The reflectivity spectral shape sensitively reflects the charge-order amplitude. The differential reflectivity spectrum $\Delta R_{\rm CO-M}/R = [R_{\rm M} - R]/R$ between the metallic and charge-ordered phases exhibits a char-

acteristic spectrum for 0.5 eV $\leq \omega \leq$ 1.05 eV, where $R_{\rm M}$ and R are the reflectivity spectra for the metallic and charge-ordered phases, respectively, and ω is the photon energy. Since the THz-pulse-induced change $\Delta R/R$ of R agrees well with normalized $\Delta R_{\rm CO-M}/R$, $\Delta R/R$ in the ω range reflects the pulse-induced modulation of the charge-order amplitude. Because ferroelectric polarization is generated by the charge order, it is natural to consider that $\Delta R/R$ reflects the pulse-induced modulation of ferroelectric polarization. Yamakawa *et al.* investigated how the initial $\Delta R/R$ depends on the direction of the THz field and found that the $\Delta R/R$ is initially largest at $\theta = 27^\circ$, where θ is the angle between the electric field $\boldsymbol{E}$ of the THz pulse and the positive $b-$axis (see Fig. 1). This strongly suggests that the angle of $\bar{\boldsymbol{P}}$ with respect to the positive $b-$axis is 27°. This is consistent with the calculation of ferroelectric polarization based on density-functional theory.[49]

However, there are still open problems. The determination of the $\bar{\boldsymbol{P}}$ direction assumes that $\Delta R/R$ is a maximum when $\boldsymbol{E}$ and $\bar{\boldsymbol{P}}$ have the same direction. However, there is no direct evidence that justifies the assumption. Furthermore, the charge transfer that dominates the pulse-induced modulation of ferroelectric polarization, and the origin of the ferroelectricity of the charge-ordered phase including the direction of polarization, have not yet been revealed. To consider these problems, we theoretically investigate the dynamics induced by THz pulse excitation from numerical calculations made using the extended Hubbard model for α-(BEDT-TTF)$_2$I$_3$. The present work finds that the main features of experimental results are reproduced well by the numerical calculations. The charge transfer through the strongest b2′ bond is dominant both for the adiabatic flow of current and for THz pulse excitation, resulting in the characteristic θ dependences of $\Delta R/R$ and ΔP and the dielectric properties of the ground state.

II. MODEL

For holes on a two-dimensional anisotropic triangular lattice, we consider the quarter-filled extended Hubbard Hamiltonian given by

$$\begin{aligned} H &= \sum_{<n,m>,\sigma} \{\beta_{n,m}(t) c^\dagger_{n,\sigma} c_{m,\sigma} + h.c.\} \\ &+ U \sum_n n_{n,\uparrow} n_{n,\downarrow} + \sum_{<n,m>} V_{n,m} n_n n_m. \end{aligned} \tag{1}$$

The first term describes the hole transfer between neighboring sites, where $c^{\dagger}_{n,\sigma}$ ($c_{n,\sigma}$) creates (annihilates) a hole of spin σ at site n, $\beta_{n,m}(t)$ is the transfer integral between sites n and m at time t, and $< n, m >$ denotes a pair of neighboring sites. The explicit formula for $\beta_{n,m}(t)$ is given later. The second term describes the on-site Coulomb interaction, where U is the on-site Coulomb interaction energy and $n_{n,\sigma} = c^{\dagger}_{n,\sigma} c_{n,\sigma}$. The third term describes the Coulomb interaction between neighboring sites, where $V_{n,m}$ is the Coulomb interaction energy for sites n and m, and $n_n = \sum_\sigma n_{n,\sigma}$. To take account of strong correlations, we calculate the exact dynamics of the THz-pulse excited state on a small cluster. We consider the 4×4 cluster (system size $N = 16$) shown in Fig. 1; a periodic boundary condition is used. We assume that $V_{n,m} = V_{\rm V}$ ($V_{\rm D}$) if the pair of neighboring sites $< n, m >$ is on vertical (diagonal) bonds.

The current operator for bond Y (Y=a1, a1$'$, $\cdots$, or b4$'$) is defined by

$$\hat{i}_{\rm Y}(t) = \hat{i}_{m,n}(t) = ie \sum_\sigma (\beta_{n,m}(t) c^{\dagger}_{n,\sigma} c_{m,\sigma} - \beta_{m,n}(t) c^{\dagger}_{m,\sigma} c_{n,\sigma}). \tag{2}$$

Here, sites n and m are connected by bond Y and satisfy the condition $\boldsymbol{r}_{n,m} \cdot \hat{\boldsymbol{e}}_b > 0$ ($\boldsymbol{r}_{n,m} \cdot \hat{\boldsymbol{e}}_a > 0$) if Y is a diagonal (vertical) bond, where $\boldsymbol{r}_{m,n}$ is a bond vector from site n to site m and the unit vector $\hat{\boldsymbol{e}}_a$ ($\hat{\boldsymbol{e}}_b$) points in the positive a (b) direction. The positive current direction through a diagonal (vertical) bond is therefore from left to right (from bottom to top) in Fig. 1. It is easily shown from the Heisenberg equation of the charge density operator that the equation of charge conservation is satisfied with the current operator.

III. RESULTS

The transfer integrals for the charge-ordered phase are deduced from the extended Hückel calculation: $\beta^{\rm (CO)}_{\rm a1} = 0.0308$, $\beta^{\rm (CO)}_{\rm a1'} = 0.0495$, $\beta^{\rm (CO)}_{\rm a2} = 0.0544$, $\beta^{\rm (CO)}_{\rm a3} = -0.0329$, $\beta^{\rm (CO)}_{\rm b1} = -0.1212$, $\beta^{\rm (CO)}_{\rm b1'} = -0.1652$, $\beta^{\rm (CO)}_{\rm b2} = -0.1577$, $\beta^{\rm (CO)}_{\rm b2'} = -0.1773$, $\beta^{\rm (CO)}_{\rm b3} = -0.0673$, $\beta^{\rm (CO)}_{\rm b3'} = -0.0656$, $\beta^{\rm (CO)}_{\rm b4} = -0.0039$, and $\beta^{\rm (CO)}_{\rm b4'} = -0.0323$,[44] where the transfer integral $\beta^{\rm (CO)}_{n,m}$ for bond b1 is denoted $\beta^{\rm (CO)}_{\rm b1}$. Those at the other bonds and other quantities are denoted in the same manner. Hereinafter, we use eV as the unit of energy and its reciprocal as the unit of time, where 1 eV^{-1} is equal to 0.658 fs. We adopt these transfer integrals for the electronic Hamiltonian $H_{\rm e}$ without electron–light interaction. In other words, $\beta_{\rm Y}(t) = \beta^{\rm (CO)}_{\rm Y}$ holds for $H_{\rm e}$.

We calculate the ground state $|\phi_0\rangle$ for $H_{\rm e}$ using the Lanczos method with various Coulomb parameters, and calculate the charge density

$$\bar{\rho}_n = \langle\phi_0|n_n|\phi_0\rangle. \tag{3}$$

We adopt Coulomb parameters that reproduce experimentally obtained charge densities well: U =0.9, $V_{\rm V}$ =0.44, and $V_{\rm D}$ =0.40. The calculated charge densities for the charge-ordered ground state are $\bar{\rho}_{\rm A}$ =0.81, $\bar{\rho}_{\rm A'}$ =0.28, $\bar{\rho}_{\rm B}$ =0.70, and $\bar{\rho}_{\rm C}$ =0.22, and the experimentally obtained charge densities in the charge-ordered phase are $\bar{\rho}_{\rm A}$ =0.82, $\bar{\rho}_{\rm A'}$ =0.29, $\bar{\rho}_{\rm B}$ =0.73, and $\bar{\rho}_{\rm C}$ =0.26.[44] The charge density $\bar{\rho}_n$ at site A is denoted $\bar{\rho}_{\rm A}$ while densities at the other sites and other quantities are denoted in the same manner.

A. Electronic polarization of the charge-ordered ground state

In this section, we calculate the electronic contribution to the electric polarization (electronic polarization) per unit cell $\bar{\boldsymbol{P}}$ of the charge-ordered ground state. It is emphasized that $\bar{\boldsymbol{P}}$ cannot be determined from the charge distribution in the unit cell but can be determined from the adiabatic flow of current.[53–56] Using the approximation based on density functional theory (DFT), the current can be calculated from the Berry phase,[53,54,57] and different methods have been proposed .[58,59] This paper directly calculates the current for the many-body wave function to fully consider the strong correlation effect.

We introduce an adiabatic parameter λ and consider the Hamiltonian $H_{\rm AC}(\lambda)$ with the transfer integrals

$$\beta_{\rm Y}(\lambda) = \lambda\beta_{\rm Y}^{\rm (CO)} + (1-\lambda)\beta_{\rm Y}^{\rm (M)}. \tag{4}$$

Here, $\beta_{\rm Y}^{\rm (M)}$ denotes the transfer integral for the metallic phase deduced from the extended Hückel calculation: $\beta_{\rm a1}^{\rm (M)} = \beta_{\rm a1'}^{\rm (M)} = 0.035$, $\beta_{\rm a2}^{\rm (M)} = 0.0461$, $\beta_{\rm a3}^{\rm (M)} = -0.0181$, $\beta_{\rm b1}^{\rm (M)} = \beta_{\rm b1'}^{\rm (M)} = -0.1271$, $\beta_{\rm b2}^{\rm (M)} = \beta_{\rm b2'}^{\rm (M)} = -0.1447$, $\beta_{\rm b3}^{\rm (M)} = \beta_{\rm b3'}^{\rm (M)} = -0.0629$, and $\beta_{\rm b4}^{\rm (M)} = \beta_{\rm b4'}^{\rm (M)} = -0.0245$.[44] The Hamiltonian $H_{\rm AC}(0)$ has inversion symmetry, and $H_{\rm AC}(1) = H_{\rm e}$ holds. The ground state of $H_{\rm AC}(\lambda)$ is denoted $|\Phi_0(\lambda)\rangle$.

We adiabatically change $\lambda(t)$ from 0 to 1 with large time interval T by assuming the relation $\lambda(t) = t/T$, and solve the time-dependent Schrödinger equation

$$i\frac{\partial}{\partial t}|\Psi(t)\rangle = H_{\rm AC}(\lambda(t))|\Psi(t)\rangle, \tag{5}$$

with the initial condition $|\Psi(0)\rangle = |\Phi_0(0)\rangle$. As T increases, the solution $|\Psi(t)\rangle$ converges to $|\Phi_0(\lambda(t))\rangle$. The used time interval (T =6000 eV^{-1}) is large enough that the differences in the charge densities between $|\Psi(t)\rangle$ and $|\Phi_0(\lambda(t))\rangle$ are less than 1%.

The net charge $\Delta Q_{\rm Y}(\lambda)$ that transfers through bond Y when the adiabatic parameter increases from zero to λ is given by the time integration of the adiabatic current flow as

$$\Delta Q_{\rm Y}(\lambda) = T\int_0^\lambda \bar{i}_{\rm Y}(T\lambda')d\lambda', \tag{6}$$

where

$$\bar{i}_{\rm Y}(t) = \langle\Psi(t)|\hat{i}_{\rm Y}(t)|\Psi(t)\rangle. \tag{7}$$

As seen from the definition of $\hat{i}_{\rm Y}$, $\Delta Q_{\rm Y}(\lambda) > 0$ holds when charge is transferred from left to right (from bottom to top) in Fig. 1 for a diagonal (vertical) bond. Because $H_{\rm AC}(0)$ has inversion symmetry, the electronic polarization is zero for $|\Phi_0(0)\rangle$. On this basis, the electronic polarization $\bar{\boldsymbol{P}}(\lambda(t))$ for $|\Phi_0(\lambda(t))\rangle$ is obtained from $\Delta Q_{\rm Y}(\lambda)$ as

$$\begin{aligned}\bar{P}_a(\lambda(t)) &= a\sum_{\rm Y}\sin(\theta_{\rm Y})\Delta Q_{\rm Y}(\lambda),\\ \bar{P}_b(\lambda(t)) &= a\sum_{\rm Y}\cos(\theta_{\rm Y})\Delta Q_{\rm Y}(\lambda),\end{aligned} \tag{8}$$

where $\bar{P}_b(\lambda(t))$ ($\bar{P}_a(\lambda(t))$) is $b-$axis ($a-$axis) component of $\bar{\boldsymbol{P}}(\lambda(t))$, $\theta_{\rm Y} = 30^\circ$ holds for bonds b2, b2$'$, b4, and b4$'$, $\theta_{\rm Y} = -30^\circ$ holds for bonds b1, b1$'$, b3, and b3$'$, and $\theta_{\rm Y} = 90^\circ$ holds for bonds a1, a1$'$, a2, and a3. Here, an equilateral-triangle lattice with lattice spacing a is assumed for simplicity. The electronic polarization of the charge-ordered ground state is given by $\bar{\boldsymbol{P}} = \bar{\boldsymbol{P}}(1)$. As T increases to 6000 eV^{-1}, $\bar{P} = |\bar{\boldsymbol{P}}|$ converges to $0.27ea$ within error of 1%. Adopting the average lattice spacing $a = 7.0$ Å, which is the length of a dominant diagonal bond,[44] and using a unit cell volume of 1639.5 Å^3,[44] we obtain $\bar{P} = 1.8\mu$C/cm^2. This value is consistent with that calculated from the Berry phase using the DFT (1.2μC/cm^2).[49] Furthermore, the angle $\theta_{\bar{\boldsymbol{P}}}$ of $\bar{\boldsymbol{P}}$ from the positive $b-$axis is 36° as shown in Fig. 2, and $\bar{\boldsymbol{P}}$ is not parallel to the $a-$axis. The numerically obtained angle $\theta_{\bar{\boldsymbol{P}}} = 36^\circ$ is consistent with the experimental result ($\theta_{\bar{\boldsymbol{P}}} = 27^\circ$) and the previous theoretical result ($\theta_{\bar{\boldsymbol{P}}} = 16^\circ$) based on DFT.[49] The difference between the present numerically obtained angle and the experimentally obtained angle is attributed mainly to the difference between equilateral-triangle lattice considered here and the real lattice structure. This point will be mentioned later.

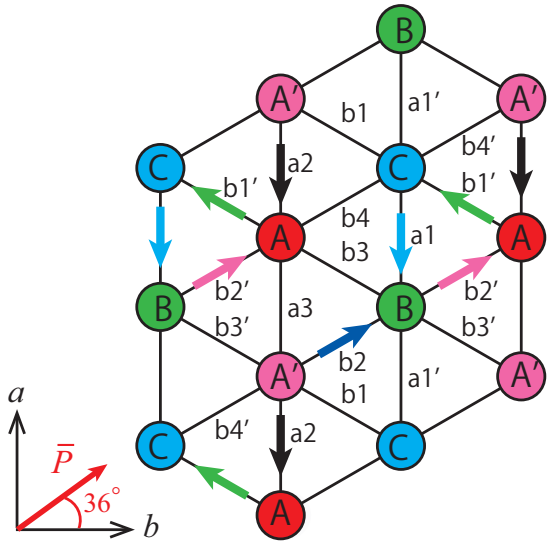

FIG. 2: (Color online) Direction of charge transfer for the five largest bonds by $|\Delta Q_{\rm Y}(\lambda)|$, and the direction of electronic polarization $\bar{\boldsymbol{P}}$ of the charge-ordered ground state.

To understand the direction of $\bar{\boldsymbol{P}}$, we consider charge transfer $\Delta Q_{\rm Y}(T)$ through each bond and the change in charge density from that of the symmetric initial state $|\Phi_0(0)\rangle$ given by

$$\Delta\bar{\rho}_n(\lambda) = \bar{\rho}_n(\lambda) - \bar{\rho}_n(0), \tag{9}$$

where

$$\bar{\rho}_n(\lambda) = \langle\Phi_0(\lambda)|n_n|\Phi_0(\lambda)\rangle. \tag{10}$$

From charge conservation, $\Delta\bar{\rho}_n(\lambda)$ is given using $\Delta Q_{\rm Y}(\lambda)$. For example, $\Delta\bar{\rho}_n(\lambda)$ at site A is given as

$$\Delta\bar{\rho}_{\rm A}(\lambda) = \frac{1}{e}[\Delta Q_{\rm a3}(\lambda) + \Delta Q_{\rm b1'}(\lambda) + \Delta Q_{\rm b2'}(\lambda) - \Delta Q_{\rm a2}(\lambda) - \Delta Q_{\rm b3}(\lambda) - \Delta Q_{\rm b4}(\lambda)]. \tag{11}$$

Here we use the fact that the A site is connected by bonds a2, a3, b1′, b2′, b3, and b4 as seen from the bond structure shown in Fig. 2. We show the λ dependence of $\Delta\bar{\rho}_{\rm X}(\lambda)$, where X =A, A′, B, or C, and $\bar{P}_b(\lambda)$ and $\bar{P}_a(\lambda)$ in Figs. 3 (a) and (c), respectively.

The relation $\bar{\rho}_{\rm A}(0) = \bar{\rho}_{\rm A'}(0)$ holds for the initial state $|\Phi_0(0)\rangle$ with the inversion symmetry. As λ increases, $\Delta\bar{\rho}_{\rm A}(\lambda)$ increases and $\Delta\bar{\rho}_{\rm A'}(\lambda)$ decreases appreciably, and the symmetric state changes to the charge-ordered ground state $|\phi_0\rangle$ without symmetry, where sites A and

B (A′ and C) are charge rich (charge poor) and a horizontal charge order is generated. As mentioned in the previous sections, electronic polarization cannot be determined from the charge distribution in the unit cell.[53–56] The dominant changes in the charge densities at sites A and A′ do not show that $\bar{\boldsymbol{P}}$ is nearly parallel to the $a-$axis.

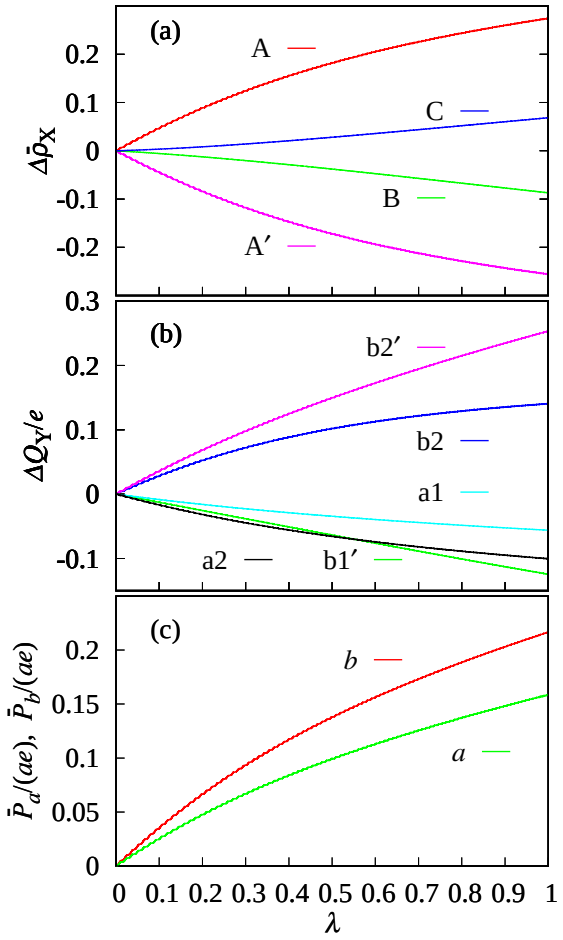

FIG. 3: (Color online) λ dependence of (a) $\Delta\bar{\rho}_X(\lambda)$, (b) $\Delta Q_Y(\lambda)$ for Y=b2′, b2, b1′, a2, and a1, and (c) $\bar{P}_b(\lambda(t))$ and $\bar{P}_a(\lambda(t))$.

We next consider the origin of the changes in charge density. Because V_V is larger than V_D, the vertical charge-ordered states have greater Coulomb interaction energies than the horizontal and diagonal charge-ordered states, and the horizontal and diagonal charge-ordered states are degenerate in terms of the Coulomb interaction energy. Bonds form between the neighboring sites as a result of charge fluctuations induced by the transfer term even in the charge-ordered states. The energy gain arising from the formation of bond Y is

given by $-\beta_{\rm Y}(\lambda)\bar{p}_{\rm Y}(\lambda)$, where

$$\bar{p}_{n,m}(\lambda) = {\rm Re}[\langle\Phi_0(\lambda)\rangle| \sum_{\sigma} c^{\dagger}_{n,\sigma} c_{m,\sigma} |\Phi_0(\lambda)\rangle] \tag{12}$$

is the bond order for $|\Phi_0(\lambda)\rangle$ and $|\bar{p}_{n,m}(\lambda)|$ is the magnitude of the bond. The degeneracy between the horizontal and diagonal charge-ordered states is lifted by the energy gain, and the charge distribution is mainly determined from the bond structure.[60–62]

To maximize the energy gain, $\bar{p}_{n,m}(\lambda)$ is larger for the bond with larger $|\beta_{\rm Y}(\lambda)|$. The absolute values $|\beta_{\rm Y}(\lambda)|$ and therefore the energy gains for bonds b1, b1$'$, b2, and b2$'$, shown by thick lines in Fig. 1, are much larger than those for other bonds. As a result, the charge distribution is mainly determined from $|\beta_{\rm Y}(\lambda)|$ for these four dominant bonds as will be shown later. As seen from Fig. 1, site A is connected by bonds b1$'$ and b2$'$, site A$'$ is connected by bonds b1 and b2, site B is connected by bonds b2 and b2$'$, and site C is connected by bonds b1 and b1$'$. At $\lambda = 1$, $|\beta_{\rm b2'}(1)| \gg |\beta_{\rm b2}(1)| \simeq |\beta_{\rm b1'}(1)| \gg |\beta_{\rm b1}(1)|$ holds. Because the holes that contribute to the stronger bonds are more stable, sites A and B (A$'$ and C), which are (are not) connected by the strongest bond b2$'$, become charge rich (charge poor), and the horizontal charge order is generated in the ground state $|\phi_0\rangle$. At $\lambda = 0$, $|\beta_{\rm b2}(0)| = |\beta_{\rm b2'}(0)| \gg |\beta_{\rm b1}(0)| = |\beta_{\rm b1'}(0)|$ holds. As a result, site B (C) is charge rich (charge poor), and $\bar{\rho}_{\rm A}(0) = \bar{\rho}_{\rm A'}(0) \simeq 0.5$ holds for the symmetric initial state. As λ increases from 0 to 1, $|\beta_{\rm b2'}(\lambda)|$ and $|\beta_{\rm b1'}(\lambda)|$ increase, and $|\beta_{\rm b2}(\lambda)|$ and $|\beta_{\rm b1}(\lambda)|$ decrease, which results in the charge transfer from site A$'$ to site A.

The five bonds with the largest $|\Delta Q_{\rm Y}(1)|$ are bonds b2$'$, b2, b1$'$, a2, and a1 in descending order. We show $\Delta Q_{\rm Y}(\lambda)$ for these five bonds in Fig. 3 (b) and their charge transfer directions in Fig. 2. The absolute values $|\Delta Q_{\rm Y}(T)|$ for bonds a2 and a3 are much smaller than those for bonds b2$'$ and b2. The indirect charge transfer A$'$→B→A along the path that consists of bonds b2$'$ and b2 with the largest and second largest $|\beta_{\rm Y}(\lambda)|$ is dominant whereas the direct transfer A$'$→A through bond a2 and that through bond a3 are not. As a result, $\bar{\boldsymbol{P}}$ is nearly parallel to bonds b2$'$ and b2. The direction of $\bar{\boldsymbol{P}}$ is mainly determined from the anisotropy of the transfer integrals.

B. THz-pulse-induced dynamics

This section shows the time variation in charge density and electronic polarization induced by a THz pulse. We consider the excitation produced by a half-cycle THz pulse. This pulse is described by a vector potential $\boldsymbol{A}(t)$ at time t given by

$$\boldsymbol{A}(t) = \hat{\boldsymbol{A}}\frac{A^{(\max)}}{2}\{1+\tanh(\frac{t}{D})\}, \tag{13}$$

where $A^{(\max)}$ is the maximum amplitude, D is the pulse duration, and $\hat{\boldsymbol{A}}$ is the unit polarization vector. The electric field of the pulse is given by

$$\begin{aligned} \boldsymbol{E}(t) &= -\hat{\boldsymbol{A}}E(t) \\ E(t) &= \frac{1}{2D}A^{(\max)}\cosh^{-2}(\frac{t}{D}). \end{aligned} \tag{14}$$

We adopt the duration $D = 300$, where the full-width at half-maximum (330 fs) is about the same as that used in the experiment, and consider the weak-excitation case $eaA^{(\max)} = 0.001$, where e is the elementary charge.

In the Hamiltonian $H(t)$ coupled with the field of the THz pulse, the electron–field coupling has been introduced into the transfer integrals as a Peierls phase, and $\beta_{n,m}(t)$ is given by

$$\beta_{n,m}(t) = \beta_{n,m}^{(\mathrm{CO})}\exp[-ie\boldsymbol{r}_{n,m}\cdot\boldsymbol{A}(t)]. \tag{15}$$

The THz-pulse-excited state $|\psi(t)\rangle$ at time t is obtained by numerically solving the time-dependent Schrödinger equation

$$i\frac{\partial}{\partial t}|\psi(t)\rangle = H(t)|\psi(t)\rangle, \tag{16}$$

with the initial condition $|\psi(-\infty)\rangle = |\phi_0\rangle$.

The time variation of charge density $\Delta\rho_n(t)$ induced by the THz pulse excitation is given by

$$\Delta\rho_n(t) = \langle\psi(t)|n_n|\psi(t)\rangle - \bar{\rho}_n. \tag{17}$$

The time variation of the electronic polarization per unit cell $\boldsymbol{\Delta P}(t) = \boldsymbol{P}(t) - \bar{\boldsymbol{P}}$ induced by the THz pulse excitation, where $\boldsymbol{P}(t)$ is the electronic polarization for $|\psi(t)\rangle$, is given

by the time integration of current flow. The net charge transfer $\Delta q_{\rm Y}(t)$ through bond Y induced by THz pulse excitation is given by

$$\Delta q_{\rm Y}(t) = \int_{-\infty}^{t} i_{\rm Y}(\tau) d\tau, \tag{18}$$

where

$$i_{\rm Y}(t) = \langle \psi(t) | \hat{i}_{\rm Y}(t) | \psi(t) \rangle. \tag{19}$$

The sign of $\Delta q_{\rm Y}(t)$ is determined so that $\Delta q_{\rm Y}(t) > 0$ holds when charge is transferred from left to right (from bottom to top) in Fig. 1 for a diagonal (vertical) bond as in the case of adiabatic current. The a [b]-component $\Delta P_a(t)$ [$\Delta P_b(t)$] of $\boldsymbol{\Delta P}(t)$ is given by

$$\begin{aligned} \Delta P_a(t) &= a \sum_{\rm Y} \sin(\theta_{\rm Y}) \Delta q_{\rm Y}(t), \\ \Delta P_b(t) &= a \sum_{\rm Y} \cos(\theta_{\rm Y}) \Delta q_{\rm Y}(t). \end{aligned} \tag{20}$$

The time variation of charge density, for example, at site A, is given using $\Delta q_{\rm Y}(t)$ as

$$\Delta \rho_{\rm A}(t) = \frac{1}{e} [\Delta q_{\rm a3}(t) + \Delta q_{\rm b1'}(t) + \Delta q_{\rm b2'}(t) - \Delta q_{\rm a2}(t) - \Delta q_{\rm b3}(t) - \Delta q_{\rm b4}(t)]. \tag{21}$$

As mentioned before, the THz-pulse-induced reflectivity change $\Delta R/R$ reflects the pulse-induced modulation of the charge-order amplitude.[49] Since charge-order generation results in the charge disproportionation between A and A$'$ sites, $\Delta \rho_{\rm A}(t) - \Delta \rho_{\rm A'}(t)$ can be regrded as the quantity that shows the pulse-induced modulation of the charge-order amplitude. The charge density changes $\Delta \rho_{\rm A}(t)$ and $\Delta \rho_{\rm A'}(t)$ are the quantities that can be directly compared with $\Delta R/R$. Since the THz-pulse-induced changes $\Delta I_{\rm SHG}/I_{\rm SHG}$ of the SHG intensity originates from the pulse-induced modulation of ferroelectric polarization, $\Delta P(t) = |\boldsymbol{P}(t)| - |\bar{\boldsymbol{P}}|$ can be directly compared with $\Delta I_{\rm SHG}/I_{\rm SHG}$. Furthermore, because ferroelectric polarization is generated by the charge order, $\Delta R/R$ also reflects $\Delta P(t)$.

As shown in the Appendix, the adiabatic approximation holds well for $|\psi(t)\rangle$ with the present parameters, and the finite-size effect in the zeroth-order term of ϵ, where ϵ is a small parameter of the adiabatic approximation, seriously affects these quantities, which are the first-order terms of ϵ. We therefore show $\Delta \rho_n(t)$ and $\Delta P_x(t)$ ($x = a$ or b) calculated using Eqs. (39) and (40), where the finite-size effect is removed, in the following.

We show in Fig. 4 the time profiles of (a) $\Delta \rho_{\rm X}(t)$ and (c) $\Delta P_x(t)$ for $\theta = 230^\circ$, where θ is the angle between $\boldsymbol{E}(t)$ and the positive $b-$axis (see Fig. 1). The four bonds with the

largest $|\Delta q_{\rm Y}(t)|$ are bonds b2′, b1′, b1, and a1 in descending order for $\theta = 230°$, and we show $\Delta q_{\rm Y}(t)$ for these four bonds in Fig. 4 (b). There are almost linear relationships between $\Delta\rho_{\rm X}$ and $E(t)$, between $\Delta P_x(t)$ and $E(t)$, and between $\Delta q_{\rm Y}(t)$ and $E(t)$, showing that these variables respond to the electric field instantaneously. These almost linear relationships hold irrespective of the polarization direction θ, resulting in the good reproduction of an important experimental result that both initial $\Delta R/R$ and $\Delta I_{\rm SHG}/I_{\rm SHG}$ are reproduced well by the THz waveform.[49] The instantaneous charge and dielectric response results from the adiabatic nature of $|\psi(t)\rangle$ as in the case of TTF-CA[63] as shown in the Appendix.

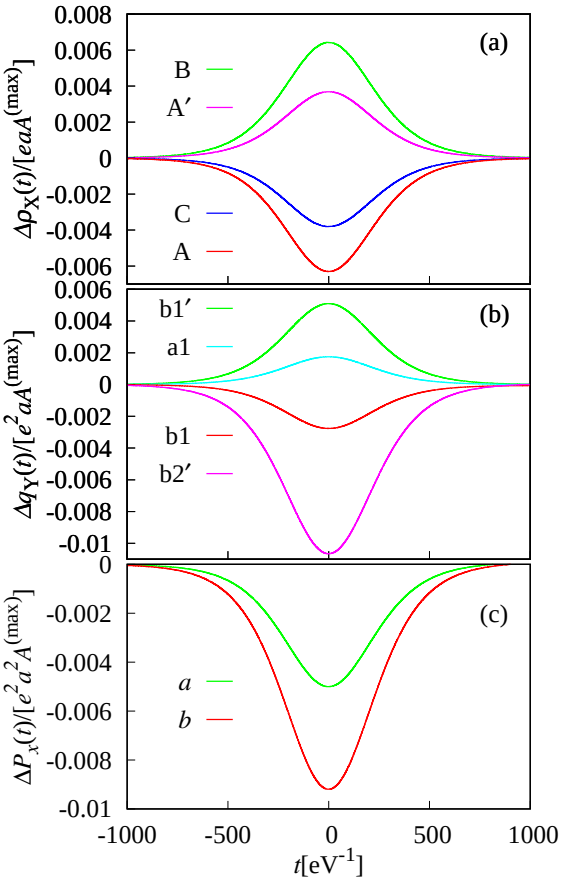

FIG. 4: (Color online) Time profiles of (a) $\Delta\rho_{\rm X}(t)$, (b) $\Delta q_{\rm Y}(t)$ for bonds b2′, b1′, b1, and a1, and (c) $\Delta P_a(t)$ and $\Delta P_b(t)$ at $\theta = 230°$.

We next consider how the THz-pulse-induced dynamics change with θ, which can be seen from the θ dependence of the peak values of the considered physical quantities because of the linear relationships. We show the θ dependences of the peak values $\Delta\rho_{\rm X}(0)$, $\Delta P(0)$, and $\Delta q_{\rm Y}(0)$ in Fig. 5, and compare the θ dependence of $\Delta R/R$ at ω =0.65 eV, where $\Delta R_{\rm CO-M}/R$

is a maximum, and at the delay time $t_{\rm d} = 0$ experimentally obtained in Ref. 49 with the θ dependence of $\Delta\rho_{\rm X}(0)$ [$\Delta P(t)$] in Fig. 5 (a) [(c)].

We consider a function $S\cos(\theta - \Theta)$ and calculate the constants S and $-90^\circ < \Theta \leq 90^\circ$ that best fit the θ dependences of $\Delta P(0)$, $\Delta\rho_{\rm X}(0)$, $\Delta q_{\rm Y}(0)$, and $\Delta R/R$, which are respectively denoted $\Delta P^{(\max)}(0)$ and Θ_P, $\Delta\rho_{\rm X}^{(\max)}(0)$ and $\Theta_{\rm X}$, $\Delta q_{\rm Y}^{(\max)}(0)$ and $\Theta_{\rm Y}$, and $(\Delta R/R)^{(\max)}$ and Θ_R. We give these values in Table I.

TABLE I: $\Delta P^{(\max)}(0)$, Θ_P, $\Delta\rho_{\rm X}^{(\max)}(0)$, $\Theta_{\rm X}$, $\Delta q_{\rm Y}^{(\max)}(0)$, $\Theta_{\rm Y}$, $(\Delta R/R)^{(\max)}$, and Θ_R

$\Delta P^{(\max)}(0)/(e^2a^2A^{(\max)})$	0.0104		$(\Delta R/R)^{(\max)}$	0.00539
Θ_P [deg]	32.6		Θ_R [deg]	26.8
X	A	A′	B	C
$\Delta\rho_{\rm X}^{(\max)}(0)/(eaA^{(\max)})$	0.00632	-0.00369	-0.00728	0.00541
$\Theta_{\rm X}$ [deg]	26.3	30.3	58.0	75.3
Y	b1	b1′	b2′	a1
$\Delta q_{\rm Y}^{(\max)}(0)/(e^2aA^{(\max)})$	0.00277	-0.00780	0.0115	-0.00216
$\Theta_{\rm Y}$ [deg]	31.2	79.2	52.4	66.1

We show the fitting curves in Fig. 5. The fitting curves reproduce the numerical results almost exactly, and the experimental data of $\Delta R/R$ are reproduced well by the fitting curve. The relations $\Theta_R \simeq \Theta_{\rm A}$ and $\Theta_R \simeq \Theta_{\rm A'}$ hold, showing that the characteristic θ dependence of $\Delta R/R$ is reproduced well by our numerical result. Furthermore, Θ_P, $\Theta_{\rm A}$, and $\Theta_{\rm A'}$ are nearly equal, showing that there exists strong positive correlation between the change of the charge-order amplitude $[\Delta\rho_{\rm A}(0) - \Delta\rho_{\rm A'}(0)]$ and the change of ferroelectric polarization magnitude $[\Delta P(0)]$. The relation $\Theta_P \simeq \theta_{\bar{\boldsymbol{P}}}$ holds, and ΔP is therefore largest (smallest) when the electric field $\boldsymbol{E}(t)$ of the THz pulse and the electronic polarization $\bar{\boldsymbol{P}}$ of the charge-ordered ground state have approximately the same (opposite) directions. In Ref. 49, the direction $\theta_{\bar{\boldsymbol{P}}}$ of ferroelectric polarization is obtained based on the assumption that the relation $\theta_{\bar{\boldsymbol{P}}} \simeq \Theta_R$ holds. This assumption is justified by the present numerical result, and this most important experimental result can be interpreted on this basis.

In the present formalism based on the time-evolution calculations, the physical quantities of interest $\boldsymbol{\Delta P}(t)$ and $\Delta\rho_n(t)$ are both given by the charge transfer $\Delta q_{\rm Y}(t)$ for each bond,

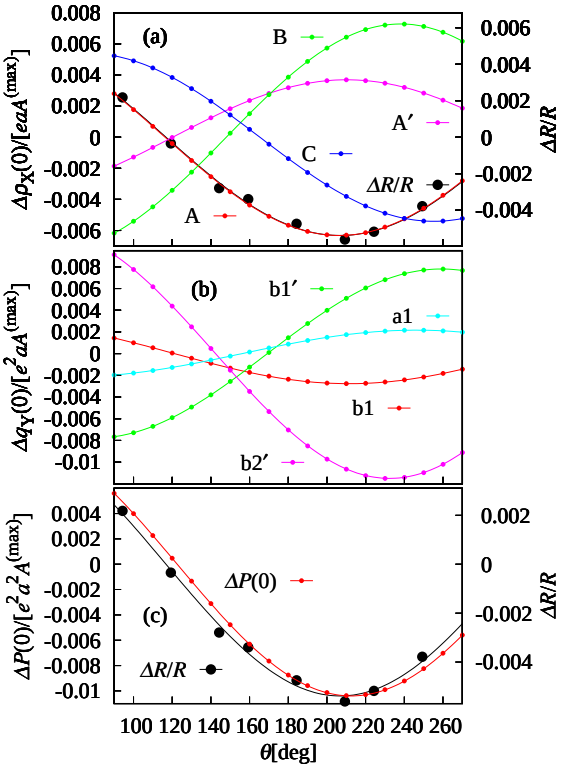

FIG. 5: (Color online) θ dependences of (a) $\Delta\rho_{\rm X}(0)$ and $\Delta R/R$ at $t_{\rm d}=0$, (b) $\Delta q_{\rm Y}(0)$ for Y=b2′, b1′, b1, and a1, and (c) $\Delta P(0)$ and $\Delta R/R$ at $t_{\rm d}=0$ (dotted lines) and fitting curves (solid lines).

which provides an important view into the origin of the ferroelectricity of the charge-ordered phase, and the origin of the characteristic θ dependence of THz-pulse induced dynamics, as will be shown later. The absolute value $|\Delta q_{\rm Y}(0)|$ is largest for bonds b2′, b1′, b2, and a1 in descending order in most of the θ region. We show the θ dependence of $\Delta q_{\rm Y}(0)$ for these four bonds in Fig. 5 (b). The absolute value $|\Delta q_{\rm b2'}(0)|$ is larger than absolute values for the other bonds in most of the θ region. Furthermore, $|\Theta_{\rm Y}-\theta_{\rm Y}|$ for bond b2′ is much smaller than those for the other bonds. This shows that $\Delta q_{\rm b2'}(0)$ is roughly proportional to the component of $\boldsymbol{E}(0)$ along the direction of bond b2′ ($E_{\rm b2'}$), but this holds only for bond b2′. For example, in the case of bond b1′ with the second largest $|\Delta q^{(\rm max)}_{\rm b1'}(0)|$, $\Theta_{\rm b1'}=79.2^\circ$ is far from $\theta_{\rm b1'}=150^\circ$. We show the charge transfer directions of these four bond at $\theta=210^\circ$ in Fig. 6. The direction of charge transfer through bond b1′ is toward the side opposite the electric field. These results show that the charge transfer from site A to site B through bond b2′ is induced by the electric field, but charge that transfers through other bonds are induced to compensate for the excess charge at site B and the deficient charge at site A

generated by the charge transfer through bond b2′.

The difference between $\Theta_{\mathrm{b2'}}$ and $\theta_{\mathrm{b2'}}$ can be attributed to the compensation. For $\theta = 210°$, $|E_{\mathrm{b2'}}|$ is the largest, but charge compensation is prohibited by the electric field $\boldsymbol{E}(t)$. As θ increases from 210° to 240°, both $|E_{\mathrm{b2'}}|$ and $|E_{\mathrm{b1'}}|$ decrease, with the decrease in the latter being greater than that in the former. The charge transfer $\Delta q_{\mathrm{b1'}}(0)$ is increased by the larger decrease in $|E_{\mathrm{b1'}}|$, and this increases $|\Delta q_{\mathrm{b2'}}(0)|$. As a result, $|\Delta q_{\mathrm{b2'}}(0)|$ is largest not at $\theta = 210°$, where $|E_{\mathrm{b2'}}|$ is largest, but at $\theta = 232.4°$. Consequently, charge transfer through the strongest bond b2′ is dominant, and $\Delta P(t)$ is thus largest (smallest) near $\theta = \theta_{\mathrm{b2'}}$ ($\theta = \theta_{\mathrm{b2'}} + 180$).

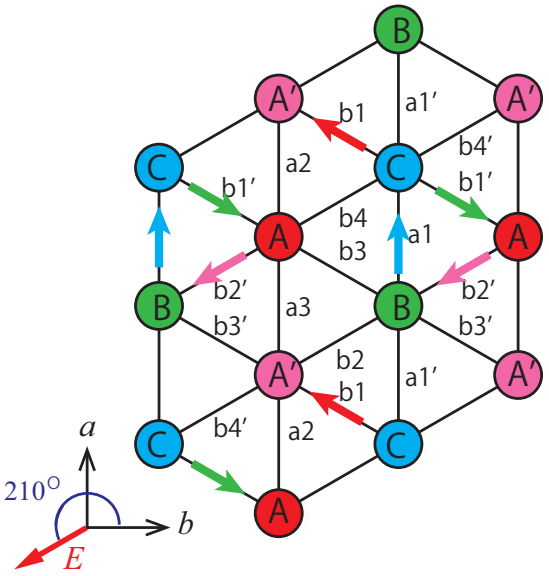

FIG. 6: (Color online) Directions of charge transfer for the four largest bonds by $|\Delta q_{\mathrm{Y}}^{(\mathrm{max})}(0)|$ shown by arrows.

IV. DISCUSSION

We discuss the implications of the present results of experimentally observed THz-pulse induced dynamics. As shown in the previous sections, the electronic polarization $\bar{\boldsymbol{P}}$ of the charge-ordered ground state is nearly parallel to bond b2′. Furthermore, the THz-pulse-induced variation in magnitude of the charge-order amplitude $|\Delta\rho_{\mathrm{A}}(t) - \Delta\rho_{\mathrm{A'}}(t)|$ and that of electronic polarization $|\Delta P(t)|$ are both largest when the polarization direction of the THz pulse is nearly parallel to bond b2′. Therefore, the direction of $\bar{\boldsymbol{P}}$ is approximately

given by the polarization direction of the THz pulse when $\Delta R/R$, which shows the THz-pulse-induced variation of the charge-order amplitude, is largest. Experimental results can be interpreted on this basis,[49] shown for the first time in this paper. This result originates from the fact that charge transfer through bond b2′ is dominant among all the bonds despite the difference between the largest transfer integral $|\beta_{\mathrm{b2'}}|$ and the second largest integral $|\beta_{\mathrm{b1'}}|$ being less than 10%.

In the present numerical calculations, an equilateral-triangle lattice is assumed, and the angle $\theta_{\mathrm{b2'}}$ between the dominant b2′ bond and $b-$axis is 30°. However, it is 23° in the real lattice. The difference $\theta_{\bar{\boldsymbol{P}}} - \theta_{\mathrm{b2'}} = 6°$ obtained in the present numerical result is very close to the experimentally obtained value of 4°. The difference in $\theta_{\bar{\boldsymbol{P}}}$ between the present theoretical and experimental results is attributed mainly to the difference in the lattice angles between these two cases.

The magnitude of the polarization change $\Delta P/\bar{P}$ is evaluated to be 1.31% from $\Delta I_{\mathrm{SHG}}/I_{\mathrm{SHG}}$, and the change in the charge-order amplitude, which corresponds to $(\Delta\rho_{\mathrm{A}} - \Delta\rho_{\mathrm{A'}})/(\bar{\rho}_{\mathrm{A}} - \bar{\rho}_{\mathrm{A'}})$, is evaluated to be 1.68% from $\Delta R/R$ for E =60 kV/cm and $\theta = 0$.[49] Our numerical results give $\Delta P/\bar{P}$ =6.5 % and $(\Delta\rho_{\mathrm{A}} - \Delta\rho_{\mathrm{A'}})/(\bar{\rho}_{\mathrm{A}} - \bar{\rho}_{\mathrm{A'}})$ =4.2 % for E = 60kV/cm and $\theta = 0$, where we adopt the average lattice spacing $a = 7$ Å and assume linear relationships between $\Delta\rho_{\mathrm{X}}$ and $E(t)$ and between $\Delta P_x(t)$ and $E(t)$. These two theoretically obtained values are comparable, which is consistent with experimental results, but these theoretically obtained values are several factors larger than those obtained experimentally. α-(BEDT-TTF)$_2$I$_3$ has a large dielectric constant.[28,47] The transfer of the valence electron makes a dominant contribution to the dielectric constant, but the other contributions that are not considered here are not negligible. The difference of several factors can be attributed to the screening of the electric field.

V. CONCLUSION

We investigated the dielectric properties of the charge-ordered phase of α-(BEDT-TTF)$_2$I$_3$ using exact numerical calculations of an extended Hubbard model. The electronic polarization $\bar{\boldsymbol{P}}$ of the charge-ordered ground state was obtained by directly calculating the current when transfer integrals were changed adiabatically from symmetric integrals to integrals for the charge-ordered phase without inversion symmetry. The angle of $\bar{\boldsymbol{P}}$ from the

positive $b-$axis was 36°, which is consistent with experimental results and previous theoretical results based on DFT. Furthermore, we numerically calculated the dynamics induced by THz pulse excitation. There are almost linear relationships between the charge density variation induced by the THz pulse $\Delta\rho_{\rm X}(t)$ and the amplitude $E(t)$ of the electric field $\boldsymbol{E}(t)$ of the pulse and between the time variation of the electronic polarization magnitude induced by the THz pulse ΔP and $E(t)$ in the case of weak excitation. These properties are found to originate from the adiabatic nature of the THz-pulse excited sate. Furthermore, the THz-pulse induced variation of charge disproportionation between A and A$'$ sites, $\Delta\rho_{\rm A}(t) - \Delta\rho_{\rm A'}(t)$, which shows the modulation of the charge-order amplitude, and $\Delta P(t)$ are largest when $\boldsymbol{E}(t)$ and $\bar{\boldsymbol{P}}$ have almost the same direction. This originates from the fact that the charge transfer through bond b2$'$ is dominant both in the adiabatic flow of current and in the THz-pulse excitation case. These results reproduce important features of experimental results of THz-pulse induced dynamics.

VI. APPENDIX

In Ref. 63, the physical properties arising from the adiabatic nature of THz-pulse excited state were shown for the one-dimensional extended Hubbard model. This result can be easily extended to the two- and three-dimensional cases as shown below.

Up to the first order of the small parameter ϵ of the adiabatic approximation, which will be explicitly given later, the solution $|\psi(t)\rangle$ of the time-dependent Schrödinger equation can be written as

$$|\psi(t)\rangle \;=\; \exp[-i\int_0^t d\tau E_0(\tau)]|\phi_0(t)\rangle + |\delta\psi(t)\rangle, \tag{22}$$

$$|\delta\psi(t)\rangle \;=\; \sum_l^{l\neq 0} c_l(t)\exp[-i\int_0^t d\tau E_l(\tau)]|\phi_l(t)\rangle, \tag{23}$$

where $|\phi_l(t)\rangle$ is the energy eigenstate of $H(t)$ with an energy eigenvalue $E_l(t)$, and $|\phi_0(t)\rangle$ and $E_0(t)$ are respectively the ground state and ground state energy. The first-order term $|\delta\psi(t)\rangle$ is given by the linear combination of $|\phi_l(t)\rangle$ with the coefficient $c_l(t)$. We divide the Hamiltonian $H(t+\Delta t)$ into the unperturbed part $H_0(t) = H(t)$ and perturbed part $H_1(t) = H(t+\Delta t) - H(t)$. Up to the first order of Δt, $H_1(t)$ can be written as

$$H_1(t) = \hat{J}(t)E(t)\Delta t, \tag{24}$$

where $\hat{J}(t)$ is given by

$$\hat{J}(t) = \sum_{<n,m>} \boldsymbol{r}_{n,m} \cdot \hat{\boldsymbol{A}} \hat{i}_{m,n}(t). \tag{25}$$

This formula for $\hat{J}(t)$ is applicable not only to the one-dimensional case but also to the two- and three-dimensional cases. Replacing the formula for $\hat{J}(t)$ given in Ref. 63 by this more general one, the results derived in Ref. 63 can be used also in the two- and three-dimensional cases. From time-dependent perturbation theory, $c_l(t)$ satisfies the differential equation

$$\frac{d}{dt} c_l(t) = \exp[i \int_0^t d\tau \omega_l(\tau)] E(t) \frac{J_{l,0}(t)}{\omega_l(t)}, \tag{26}$$

where $J_{l,0}(t)$ is the transition dipole moment given by

$$J_{l,0}(t) = \langle \phi_l(t) | \hat{J}(t) | \phi_0(t) \rangle, \tag{27}$$

and $\omega_l(t) = E_l(t) - E_0(t)$. As shown later, in the thermodynamic limit, $J_{l,0}(t)$ and $\omega_l(t)$ are constant with time, and $J_{l,0}(t) = J_{l,0}$ and $\omega_l(t) = \omega_l$ hold, where $J_{l,0}$ and ω_l are the transition dipole moment and the excitation energy when $\boldsymbol{A}(t) = 0$. We can then solve the differential equation (26) and obtain $c_l(t)$ as

$$c_l(t) = -i \frac{J_{l,0}}{\omega_l^2} \exp[i\omega_l t] E(t), \tag{28}$$

where the terms of second order or higher in $1/(\omega_l D)$ are neglected. In the case of THz pulse excitation, $1/(\Delta E D) \ll 1$ holds, where ΔE is the optical energy gap, in the charge-ordered ground state. This approximation holds well for almost all insulators. The small parameter ϵ for the adiabatic approximation is therefore given by

$$\epsilon = \max(\frac{|J_{l,0}|}{\omega_l^2}) \frac{A^{(\max)}}{D}, \tag{29}$$

and the adiabatic approximation is good if $\epsilon \ll 1$ holds.

The expectation value of, for example, charge density $\rho_n(t) = \langle \psi(t) | n_n | \psi(t) \rangle$ is expanded into a power series of ϵ as

$$\rho_n(t) = \rho_n^{(0)}(t) + \rho_n^{(1)}(t) + \cdots, \tag{30}$$

where $\rho_n^{(i)}(t)$ is the ith-order term. The zeroth- and the first-order terms are given by

$$\rho_n^{(0)}(t) = \langle \phi_0(t) | n_n | \phi_0(t) \rangle, \tag{31}$$

$$\rho_n^{(1)}(t) = 2\mathrm{Re}[\exp[i \int_0^t d\tau E_0(\tau)] \langle \phi_0(t) | n_n | \delta\psi(t) \rangle]. \tag{32}$$

Substituting Eq. (28) into Eq. (31), the first-order term is given by

$$\rho_n^{(1)}(t) = G_n eaE(t), \tag{33}$$

$$G_n = 2\mathrm{Im}[\sum_l^{l\neq 0} \frac{J_{l,0}}{\omega_l^2}\langle\phi_0|n_n|\phi_l\rangle]. \tag{34}$$

We consider the unitary transformation

$$\tilde{c}_{n,\sigma} = c_{n,\sigma}\exp[-ie\boldsymbol{r}_n\cdot\bar{A}(t)], \tag{35}$$

where $\boldsymbol{r}_n$ is the position vector of site n. When the bond connecting sites n and m does not cross the periodic boundary, $\boldsymbol{r}_{n,m} = \boldsymbol{r}_m - \boldsymbol{r}_n$ holds and it can be written as

$$\beta_{n,m}(t)c_{n,\sigma}^\dagger c_{m,\sigma} = \beta_{n,m}^{(\mathrm{CO})}\tilde{c}_{n,\sigma}^\dagger\tilde{c}_{m,\sigma}. \tag{36}$$

When the bond connecting sites n and m crosses the periodic boundary, a phase factor is added to the transfer integral. Thus, the time- and space- invariant vector potential introduces a twist in the boundary condition, but does not change $H(t)$ and $\hat{J}(t)$ except for this. The finite-size effect induced by the twist is of the order of $1/\sqrt{N}$ in the present two-dimensional case. Therefore, $\rho^{(0)}(t) = \bar{\rho}$ and $\Delta\rho_n(t) = \rho_n^{(1)}(t)$ hold up to the first order of ϵ in the thermodynamic limit. The time variation $\Delta\rho_n(t)$ is proportional to $E(t)$ in this instance.

In the present numerical calculation with the small-size cluster, the artifact $\rho^{(0)}(t) - \bar{\rho}$ caused by the finite-size effect is of zeroth order in ϵ and is therefore comparable to $\rho_n^{(1)}(t)$. It is essential to remove the artifact. We remove $\rho^{(0)}(t) - \bar{\rho}$ using the numerical method shown below. We consider the time variation of charge density induced by a pulse with renormalized duration rD given by

$$\boldsymbol{A}^{(r)}(t) = \hat{\boldsymbol{A}}\frac{A^{(\max)}}{2}\{1 + \tanh(\frac{t}{rD})\}. \tag{37}$$

Because $H^{(r)}(rt) = H(t)$ holds, where $H^{(r)}(t)$ is the Hamiltonian with the pulse described by $\boldsymbol{A}^{(r)}(t)$, the time-dependent solution $|\psi^{(r)}(t)\rangle$ of $H^{(r)}(t)$ can be written as

$$|\psi^{(r)}(rt)\rangle = \exp[-ir\int_0^t d\tau E_0(\tau)]|\phi_0(t)\rangle + |\delta\psi^{(r)}(rt)\rangle, \tag{38}$$

up to the first order of ϵ/r, where $|\delta\psi^{(r)}(t)\rangle$ is the first-order term of ϵ/r. The zeroth-order term can be removed using Eqs. (22) and (38), and $\Delta\rho_n$ is given by

$$\Delta\rho_n(t) = \frac{r}{r-1}\{\langle\psi(t)|n_n|\psi(t)\rangle - \langle\psi^{(r)}(rt)|n_n|\psi^{(r)}(rt)\rangle\}, \tag{39}$$

where the contributions from the terms higher than first order are neglected, and we use the fact that the leading term of $\langle\psi^{(r)}(rt)|n_n|\psi^{(r)}(rt)\rangle - \langle\phi_0(t)|n_n|\phi_0(t)\rangle$ is of the first order of ϵ/r, which can be derived from Eq. (33). The contributions from the terms higher than first order are negligible with the present small $eaA^{(\max)}$. This can be confirmed from the differences between the values of $\Delta\rho(t)$ calculated with $r = 2$ and 3 being less than 1%.

In the same manner, we can remove the artifact caused by the finite-size effect from electronic polarization $\boldsymbol{\Delta P}(t)$:

$$\Delta P_a(t) = a\frac{r^2}{r^2-1}\sum_{\rm Y}\sin(\theta_{\rm Y})\int_{-\infty}^{t}[\langle\psi(\tau)|\hat{i}_{\rm Y}(\tau)|\psi(\tau)\rangle - \langle\psi^{(r)}(r\tau)|\hat{i}_{\rm Y}(\tau)|\psi^{(r)}(r\tau)\rangle]d\tau,$$

$$\Delta P_b(t) = a\frac{r^2}{r^2-1}\sum_{\rm Y}\cos(\theta_{\rm Y})\int_{-\infty}^{t}[\langle\psi(\tau)|\hat{i}_{\rm Y}(\tau)|\psi(\tau)\rangle - \langle\psi^{(r)}(r\tau)|\hat{i}_{\rm Y}(\tau)|\psi^{(r)}(r\tau)\rangle]d\tau. \quad (40)$$

We here use the fact that the leading term of $\langle\psi^{(r)}(rt)|\hat{i}_{\rm Y}(t)|\psi^{(r)}(rt)\rangle - \langle\phi_0(t)|\hat{i}_{\rm Y}(t)|\phi_0(t)\rangle$ is of the second order of ϵ/r. We also check this on the basis that the difference between the values of $\Delta P_a(t)$ calculated with $r = 2$ and 3, and that of $\Delta P_b(t)$ are both less than 1%.

VII. ACKNOWLEDGMENTS

This work was supported by JSPS KAKENHI under grant number JP16K05402 and JST CREST under grant number JPMJCR1661. We thank Glenn Pennycook, MSc, from Edanz Group (www.edanzediting.com/ac) for editing a draft of this manuscript.

---

* Corresponding author: takahashi.akira@nitech.ac.jp

[1] K. Uchino, Ferroelectric Devices (Marcel Dekker, New York 2000).

[2] M. E. Lines and A. M. Glass, Principles and Applications of Ferroelectrics and Related Materials (Oxford University, New York 1977).

[3] J. F. Scott, Science **315**, 954 (2007).

[4] T. Portengen, Th. Östreich, and L. J. Sham, Phys. Rev. **B 54** 17452 (1996).

[5] J. van den Brink and D. I. Khomskii, J. Phys. Condens. Matter **20**, 434217 (2008).

[6] S. Ishihara, J. Phys. Soc. Jpn. **79**, 011010 (2010).

[7] T. Kimura, T. Goto, H. Shintani, K. Ishizaka, T. Arima, and Y. Tokura, Nature **426**, 55 (2003).

[8] J. Wang, J. B. Neaton, H. Zheng, V. Nagarajan, S. B. Ogale, B. Liu, D. Viehland, V. Vaithyanathan, D. G. Schlom, U. V. Waghmare, N. A. Spaldin, K. M. Rabe, M. Wuttig, and R. Ramesh, Science **299**, 1719 (2003).

[9] N. A. Spaldin and M. Fiebig, Science **309**, 391 (2005).

[10] W. Eerenstein, N. D. Mathur and J. F. Scott, Nature (London) **442**, 759 (2006).

[11] S.-W Cheong and M. Mostovoy, Nature Mater. **6**, 13@(2007).

[12] S. Picozzi, K. Yamauchi, B. Sanyal, I. A. Sergienko, and E. Dagotto, Phys. Rev. Lett. **99**, 227201 (2007).

[13] D. Khomskii, Physics **2**, 20 (2009).

[14] P. Lunkenheimer, J. Müller, S. Krohns, F. Schrettle, A. Loidl, B. Hartmann, R. Rommel, M. de Souza, C. Hotta, J. A. Schlueter, and M. Lang, Nature Materials **11**, 755 (2012).

[15] N. Ikeda, H. Ohsumi, K. Ohwada, K. Ishii, T. Inami, K. Kakurai, Y. Murakami, K. Yoshii, S. Mori, Y. Horibe, and H. Kito, Nature **436**, 1136 (2005).

[16] A. Nagano, M. Naka, J. Nasu, and S. Ishihara, Phys. Rev. Lett. **99**, 217202 (2007).

[17] M. Naka, A. Nagano, and S. Ishihara, Phys. Rev. B **77**, 224441 (2008).

[18] K. Kobayashi, S. Horiuchi, R. Kumai, F. Kagawa, Y. Murakami, and Y. Tokura, Phys. Rev. Lett. **108**, 237601 (2012).

[19] G. Giovannetti, S. Kumar, A. Stroppa, J. van den Brink, and S. Picozzi, Phys. Rev. Lett. **103**, 266401 (2009).

[20] S. Ishibashi and K. Terakura, Physica B (Amsterdam) **405**, S338 (2010).

[21] S. Ishibashi and K. Terakura, J. Phys. Soc. Jpn. **83** 073702 (2014).

[22] K. Terakura and S. Ishibashi, Phys. Rev. **B 91** 195120 (2015).

[23] P. Monceau, F. Ya. Nad, and S. Brazovskii, Phys. Rev. Lett. **86**, 4080 (2001).

[24] H. Yoshioka, M. Tsuchiizu, and H. Seo, J. Phys. Soc. Jpn. **76**, 103701 (2007).

[25] Y. Otsuka, H. Seo, Y. Motome, and T. Kato, J. Phys. Soc. Jpn. **77**, 113705 (2008).

[26] K. Yamamoto, S. Iwai, S. Boyko, A. Kashiwazaki, F. Hiramatsu, C. Okabe, N. Nishi, and K. Yakushi, J. Phys. Soc. Jpn. **77**, 074709 (2008).

[27] K. Yamamoto, A. Kowalska, and K. Yakushi, Appl. Phys. Lett. **96**, 122901 (2010).

[28] P. Lunkenheimer, B. Hartmann, M. Lang, J. Müller, D. Schweitzer, S. Krohns, and A. Loidl, Phys. Rev. B **91**, 245132 (2015).

[29] M. Abdel-Jawad, I. Terasaki, T. Sasaki, N. Yoneyama, N. Kobayashi, Y. Uesu, and C. Hotta,

Phys. Rev. B **82**, 125119 (2010).

[30] H. Gomi, T. Imai, A. Takahashi, and M. Aihara: Phys. Rev. **B 82**, 035101 (2010).

[31] M. Naka and S. Ishihara, J. Phys. Soc. Jpn. **79**, 063707 (2010).

[32] C. Hotta, Phys. Rev. B **82**, 241104 (2010).

[33] S. Dayal, R. T. Clay, H. Li, and S. Mazumdar, Phys. Rev. B **83**, 245106 (2011).

[34] K. Itoh, H. Itoh, M. Naka, S. Saito, I. Hosako, N. Yoneyama, S. Ishihara, T. Sasaki, and S. Iwai, Phys. Rev. Lett. **110**, 106401 (2013).

[35] M. Naka and S. Ishihara, J. Phys. Soc. Jpn. **82**, 023701 (2013).

[36] H. Gomi, M. Ikenaga, Y. Hiragi, D. Segawa, A. Takahashi, T. J. Inagaki, and M. Aihara, Phys. Rev. B **87**, 195126 (2013).

[37] H. Gomi, T. J. Inagaki, and A. Takahashi, Phys. Rev. B **93**, 035105 (2016).

[38] K. Miyagawa, A. Kawamoto, and K. Kanoda, Phys. Rev. B **62**, R7679 (2000).

[39] H. Seo, J. Phys. Soc. Jpn. **69**, 805 (2000).

[40] R. Chiba, H. Yamamoto, K. Hiraki, T. Takahashi, and T. Nakamura, J. Phys. Chem. Solids **62**, 389 (2001).

[41] M. Watanabe, Y. Noda, Y. Nogami, and H. Mori, J. Phys. Soc. Jpn. **73**, 116 (2004).

[42] Y. Takano, K. Hiraki, H. M. Yamamoto, T. Nakamura, and T. Takahashi, J. Phys. Chem. Solids **62**, 393 (2001).

[43] Y. Takano, K. Hiraki, H. M. Yamamoto, T. Nakamura, and T. Takahashi, Synth. Met. **120**, 1081 (2001).

[44] T. Kakiuchi, Y. Wakabayashi, H. Sawa, T. Takahashi, and T. Nakamura, J. Phys. Soc. Jpn. **76**, 113702 (2007).

[45] Y. Yue, K. Yamamoto, M. Uruichi, C. Nakano, K. Yakushi, S. Yamada, T. Hiejima, and A. Kawamoto, Phys. Rev. B **82**, 075134 (2010).

[46] F. Nad, P. Monceau, and H. M. Yamamoto, Phys. Rev. B **76**, 205101 (2007).

[47] T. Ivek, B. Korin-Hamzić, O. Milat, S. Tomić, C. Clauss, N. Drichko, D. Schweitzer, and M. Dressel, Phys. Rev. **B 83**, 165128 (2011).

[48] T. Miyamoto, H. Yada, H. Yamakawa, and H.i Okamoto, Nat. Commun. **4**, 2586 (2013).

[49] H. Yamakawa, T. Miyamoto, T. Morimoto, H. Yada, Y. Kinoshita, M. Sotome, N. Kida, K. Yamamoto, K. Iwano, Y. Matsumoto, S. Watanabe, Y. Shimoi, M. Suda, H. M. Yamamoto, H. Mori, and H. Okamoto, Sci. Rep. **6**, 20571 (2016).

[50] T. Ivek, I. Kovačević, M. Pinterić, B. Korin-Hamzić, S. Tomić, T. Knoblauch, D. Schweitzer, and M. Dressel, Phys. Rev. **B 86**, 245125 (2012).

[51] A. Ito, Y. Nakamura, A. Nakamura, and H. Kishida, Phys. Rev. Lett. **111**, 197801 (2013).

[52] S. Iwai, K. Yamamoto, A. Kashiwazaki, F. Hiramatsu, H. Nakaya, Y. Kawakami, K. Yakushi, H. Okamoto, H. Mori, and Y. Nishio, Phys. Rev. Lett. **98**, 097402 (2007).

[53] R. D. King-Smith and D. Vanderbilt, Phys. Rev. **B 47**, 1651 (1993).

[54] R. Resta, Rev. Mod. Phys. **66**, 899 (1994).

[55] R. E. Cohen, Nature (London) **358**, 136 (1992).

[56] T. Egami, S. Ishihara, and M. Tachiki, Science **261**, 1307 (1993).

[57] D. Vanderbilt and R. D. King-Smith, Phys. Rev. **B 48**, 4442 (1993).

[58] S. Onoda, S. Murakami, and N. Nagaosa, Phys. Rev. Lett. **93**, 167602 (2004).

[59] R. Nourafkan and G. Kotliar, Phys. Rev. **B 88**, 155121 (2013)

[60] Y. Tanaka and K. Yonemitsu, J. Phys. Soc. Jpn. **77**, 034708 (2008).

[61] S. Miyashita and K. Yonemitsu, J. Phys. Soc. Jpn. **77**, 094712 (2008).

[62] K. Oya and A. Takahashi, Phys. Rev. **B 97**, 115147 (2018).

[63] H. Gomi, N. Yamagishi, T. Mase, T. J. Inagaki, and A. Takahashi, Phys. Rev. **B 95**, 094116 (2017).